

RESEARCH ARTICLE

Cavin4b/Murcb Is Required for Skeletal Muscle Development and Function in Zebrafish

Michael P. Housley^{1,2*}, Brian Njaine², Filomena Ricciardi², Oliver A. Stone^{1,2}, Soraya Hölper², Marcus Krüger^{2a}, Sawa Kostin², Didier Y. R. Stainier^{1,2*}

1 Department of Biochemistry and Biophysics, University of California, San Francisco (UCSF), San Francisco, California, United States of America, **2** Max Planck Institute for Heart and Lung Research, Bad Nauheim, Germany

^a Current address: Institute for Genetics and Cologne Excellence Cluster on Cellular Stress Responses in Aging-Associated Diseases (CECAD), University of Cologne, Cologne, Germany.

* housley.michael@gmail.com (MPH); didier.stainier@mpi-bn.mpg.de (DYRS)



CrossMark
click for updates

 OPEN ACCESS

Citation: Housley MP, Njaine B, Ricciardi F, Stone OA, Hölper S, Krüger M, et al. (2016) Cavin4b/Murcb Is Required for Skeletal Muscle Development and Function in Zebrafish. *PLoS Genet* 12(6): e1006099. doi:10.1371/journal.pgen.1006099

Editor: Mary C. Mullins, University of Pennsylvania School of Medicine, UNITED STATES

Received: July 13, 2015

Accepted: May 10, 2016

Published: June 13, 2016

Copyright: © 2016 Housley et al. This is an open access article distributed under the terms of the [Creative Commons Attribution License](https://creativecommons.org/licenses/by/4.0/), which permits unrestricted use, distribution, and reproduction in any medium, provided the original author and source are credited.

Data Availability Statement: All relevant data are within the paper and its Supporting Information files.

Funding: The research was made possible by a grant from the California Institute for Regenerative Medicine [TG2-01153] to MPH, as well as by funds from the National Institutes of Health (RO1KL54737), Packard Foundation and Max Planck Society to DYRS. The funders had no role in study design, data collection and analysis, decision to publish, or preparation of the manuscript.

Competing Interests: The authors have declared that no competing interests exist.

Abstract

Skeletal muscles provide metazoans with the ability to feed, reproduce and avoid predators. In humans, a heterogeneous group of genetic diseases, termed muscular dystrophies (MD), lead to skeletal muscle dysfunction. Mutations in the gene encoding Caveolin-3, a principal component of the membrane micro-domains known as caveolae, cause defects in muscle maintenance and function; however it remains unclear how caveolae dysfunction underlies MD pathology. The Cavin family of caveolar proteins can form membrane remodeling oligomers and thus may also impact skeletal muscle function. Changes in the distribution and function of Cavin4/Murc, which is predominantly expressed in striated muscles, have been reported to alter caveolae structure through interaction with Caveolin-3. Here, we report the generation and phenotypic analysis of *murcb* mutant zebrafish, which display impaired swimming capacity, skeletal muscle fibrosis and T-tubule abnormalities during development. To understand the mechanistic importance of Murc loss of function, we assessed Caveolin-1 and 3 localization and found it to be abnormal. We further identified an *in vivo* function for Murc in Erk signaling. These data link Murc with developmental defects in T-tubule formation and progressive muscle dysfunction, thereby providing a new candidate for the etiology of muscular dystrophy.

Author Summary

Membrane structures are critical to skeletal muscle excitation-contraction coupling, and disruptions in key membrane proteins can lead to muscular dystrophy. Caveolae, micro-domains in the cell membrane, are known to be important in forming muscle-specific membrane structures such as the T-tubule network and play a role in some forms of muscular dystrophy. Two classes of proteins help form caveolae: Caveolins and Cavins. However, it is poorly understood how Cavins function in skeletal muscle development or

whether Cavin dysfunction can lead to muscular dystrophy. To address these questions, we generated a Cavin4b/Murcb deficient zebrafish line by targeted TALEN mutagenesis and found that Cavin4b/Murcb is necessary for the formation and function of skeletal muscle. Cavin4b/Murcb mutant zebrafish exhibit progressive skeletal muscle deterioration, disrupted membrane structures early in development and aberrant growth factor signaling. Cavin4b/Murcb deficient fish have smaller and irregularly shaped muscle fibers with fibrosis, similar to what is observed in muscular dystrophy. Cavin4b/Murcb mutant fish also exhibit mislocalized Caveolin-1 and Caveolin-3 as well as disrupted T-tubules, suggesting that Cavin4b/Murcb regulates the distribution of caveolar proteins and that this misregulation impacts the development of the T-tubule network.

Introduction

Muscular dystrophies (MD) are a heterogeneous group of genetic diseases that result in progressive dysfunction of skeletal muscle [1]. Muscle weakness and loss of muscle mass can begin in childhood, while some forms of the disease manifest in adulthood. Different groups of muscles are affected depending on the type of MD and complications can include confinement to a wheelchair, scoliosis, difficulty swallowing, impaired breathing, cardiomyopathies, and early death [2,3]. Although MD can be caused by mutations in more than 30 different genes [4], common phenotypic characteristics include disruption in the membrane network [5] and abnormal calcium flux in skeletal muscle [6,7]. Loss of membrane integrity has been shown by the intracellular accumulation of proteins normally absent in skeletal muscle [8,9]. Membrane stability requires functional costameres [10], which link intracellular force generation with the extracellular matrix [11,12] via the dystrophin glycoprotein complex [13].

Cell membrane (sarcolemma) stability is critical to muscle cells, which must maintain a resting membrane potential in order to propagate action potentials via voltage-gated ion channels [14]. Excitation-contraction coupling requires specialized membrane structures, the transverse (T)-tubules and terminal cisternae, for calcium flux to trigger an actin/myosin dependent contraction. Two terminal cisternae are found on opposing sides of the T-tubules and form a structure known as the triad [15]. Disruption of calcium signaling also has long term consequences for skeletal muscle health by altering signaling pathways required for muscle remodeling [16] and may underlie the necrosis seen in MD [6]. Interestingly, in a zebrafish model of Duchenne muscular dystrophy, a serotonin reuptake inhibitor was shown to improve skeletal muscle health through improved calcium homeostasis [17].

In mouse, the development of the T-tubule network begins with invaginations in the sarcoplasmic reticulum at embryonic day (E)15 followed by postnatal maturation of the network [15]. Thus far, a few proteins are known to be required for T-tubulogenesis: MTM1, JPH1, MG29, DYSE, BIN1, and Caveolin-3 (CAV3). Loss of MTM1 in humans results in a disease known as myotubular myopathy and is characterized by severe muscle atrophy at birth, and mice lacking MTM1 show T-tubule disorganization with disrupted calcium homeostasis and excitation-contraction coupling defects [18]. Bin1, which possesses membrane deforming properties, has been shown to be enriched at T-tubules and induce tubular invaginations in the plasma membrane [19]. Loss of CAV3 can result in several skeletal muscle diseases including type 1C limb-girdle muscular dystrophy [20]. Knockout of *Cav3* in mouse leads to disrupted dystrophin glycoprotein complex distribution as well as abnormal T-tubulogenesis [21], and Cav3 is necessary for skeletal muscle differentiation *in vitro* [22,23] and in zebrafish [24].

Primarily expressed in striated muscle, Cav3 is an integral membrane protein required for the formation of caveolae, invaginations in the cell membrane that function in lipid storage, signaling and endocytosis [25]. Caveolin-1 (Cav1), a broadly expressed member of the Caveolin family, is required for lipid homeostasis and insulin sensitivity [26]. The Caveolin proteins interact with a class of membrane-associated proteins termed Cavins, which are enriched in caveolae and are critical for their formation. The Cavin family consists of 4 members, one of which is Cavin4, also known as Murc (Muscle-restricted coiled-coil protein).

Cavin4/Murc was originally discovered through SAGE screening of a cDNA library prepared from adult mouse hearts [27] and expression analysis revealed high mRNA expression in both heart and skeletal muscles. In cultured C2C12 myoblasts, CAVIN4/MURC expression was found to increase during differentiation [28]. Additionally, shRNA-mediated knockdown of CAVIN4/MURC resulted in the inhibition of myotube formation. Concurrent with these initial studies, *Cavin4/Murc* was also identified by scanning the genome for homologs of three known Cavin genes and was thus termed “*Cavin4*” [29]. The four members of the Cavin family were found to localize to the cell membrane in a CAV1-dependent manner, and in skeletal muscle, CAVIN4/MURC co-localizes with CAV3 in putative caveolae [29]. In cardiomyocytes, CAVIN4/MURC localizes to caveolae and T-tubules and its over-expression results in disrupted caveolar shape [30]. Furthermore, in a patient with rippling muscle disease and mosaically expressed CAV3, muscle fibers lacking CAV3 had a distinct absence of CAVIN4/MURC expression [29].

The Cavin proteins possess substantial homo- and hetero-oligomerization capacity via two helical repeat (HR) domains [31]. Although their functional importance for caveolar formation is unclear, Cavins have the capacity to remodel membranes and it has been proposed that they polymerize to form large assemblies of rod-like structures stabilized by interactions with membranes [31].

Here, we report the generation of a zebrafish line carrying a TALEN-induced *murcb* mutant allele and show that Cavin4b/Murcb is necessary for skeletal muscle function in both larval and adult fish. Cavin4b/Murcb deficiency results in progressive dysfunction and fibrosis of skeletal muscles. Additionally, we show that disruption of Cavin4b/Murcb is associated with changes in Erk signaling and Caveolin expression in adult zebrafish. Larvae lacking Cavin4b/Murcb exhibit an increased number of caveolae, mislocalization of Caveolin-1 expression, and T-tubule defects.

Results

Cavin4/Murc is conserved between zebrafish and mammals and is expressed in the somites during zebrafish development

Using a combinatorial Translating Ribosome Affinity Purification (TRAP) approach, we previously found that *murca* and *murcb* are expressed in the somites of developing zebrafish [32]. To understand the function of the *murc* genes, we first examined their conservation and spatio-temporal expression pattern. We aligned the protein sequences of Cavin4a/Murca and Cavin4b/Murcb with mammalian and *Xenopus* paralogs (S1A Fig) and concluded that *murca* and *murcb* are indeed duplicated genes by examining their genomic structure (S1B Fig) and through phylogenetic analysis of the protein sequences (S1C Fig). To determine when *murca* and *murcb* are expressed, we performed RT-PCR analysis on RNA isolated from developing zebrafish embryos and larvae at various times and found that mRNA for both *murc* paralogs are detectable beginning around 29 hours post fertilization (hpf) and expressed through 128 hpf (Fig 1A). In adult tissues, we found *murca* and *murcb* to be highly expressed in skeletal muscle, and to a reduced extent, both *murc* paralogs are also expressed in the kidney (Fig 1B).

that mediate interactions with the Cavin proteins [31]. To determine whether the *s983* lesion results in altered Cavin4b/Murcb protein expression, we performed antibody staining on transverse sections of skeletal muscle harvested from 10 wpf zebrafish and found a reduction in anti-Cavin4/Murcb immunoreactivity (Fig 1E). To confirm that the *s983* homozygous mutant larvae lack Cavin4b/Murcb, we performed tandem mass spectrometry and found that peptides corresponding to Cavin4b/Murcb were not detected in lysates from mutant larvae but were clearly present in heterozygous controls (S1 Table, S2 Fig). Altogether, these data indicate that *s983* is a severe mutant allele.

Cavin4b/Murcb deficient zebrafish are smaller and have defects in skeletal muscle morphology

To characterize the phenotype of *murcb* mutant zebrafish, we examined 10 wpf mutant and siblings from in-crosses of *murcb*^{s983/+} animals and measured body mass and length and found that *murcb*^{s983/s983} fish were smaller with an average mass of 0.25 g compared to 0.46 g for *murcb*^{+/+} fish and 0.45 g for *murcb*^{s983/+} fish (Fig 2A and 2B). The average length of *murcb*^{s983/s983} animals at 24.4 mm also differed significantly from the *murcb* wild-type and heterozygous animals with average lengths of 27.7 mm and 27.9 mm, respectively.

To analyze skeletal muscle structure in *murcb* mutant fish, we harvested trunk tissue from animals sacrificed at 10 wpf and examined transverse sections histologically. Hematoxylin and eosin (H&E) staining revealed that the overall organization and symmetry of the trunk was not altered in *murcb*^{s983/s983} fish (Fig 2C) compared with sibling controls, though skeletal muscle fibers appeared smaller. F-actin visualization in these transverse sections revealed that skeletal muscle fibers were smaller and less uniform in size and shape in *murcb*^{s983/s983} fish compared to heterozygous siblings (Fig 2D). To assess the skeletal muscle pathology of Cavin4b/Murcb deficient zebrafish, we performed trichrome staining of transverse sections made from 12 mpf trunk tissue and found evidence of fibrosis in mutant animals but not in sibling controls (Fig 2E).

To determine whether there is a role for Cavin4b/Murcb during the early development of skeletal muscle structure, we initially examined *murcb*^{s983/s983} larvae at 5 dpf and found no gross morphological differences with *murcb*^{s983/+} siblings (Fig 2F). Additionally, whole mount phalloidin staining of skeletal muscle F-actin revealed no obvious differences between *murcb*^{s983/s983} larvae and *murcb*^{s983/+} siblings (Fig 3) at 3 dpf. In contrast, at 6 dpf we found that skeletal muscle fibers were smaller and less consistent in size in *murcb*^{s983/s983} larvae compared with *murcb*^{s983/+} siblings (Fig 3). To determine whether the membranes of the skeletal muscle were intact in *murcb* mutant larvae, we performed Evans blue dye staining [35], and found the somites of both heterozygous *murcb*^{s983/+} and *murcb*^{s983/s983} larvae to be impermeable to the dye (S3A Fig). In order to understand whether apoptosis was contributing to the disruption in skeletal muscle fiber size in *murcb*^{s983/s983} larvae, we performed acridine orange staining on whole mount zebrafish and found no difference between mutants and *murcb*^{s983/+} siblings (S3B Fig). Additionally, we assessed mRNA stability for both *murca* and *murcb* by RT-PCR in both *murcb*^{s983/+} and *murcb*^{s983/s983} larvae and found that transcripts for both *murca* paralogs were relatively unaffected (S3C Fig).

Cavin4b/Murcb deficient fish have reduced skeletal muscle function

To determine whether structural defects in the skeletal muscle of *murcb* mutants affect skeletal muscle function, we quantified the maximum swimming velocity and acceleration following the startle response. At 10 wpf, *murcb*^{s983/s983} fish were significantly slower with a maximum velocity of 0.473 m/s compared to their heterozygous siblings that had a maximum velocity of

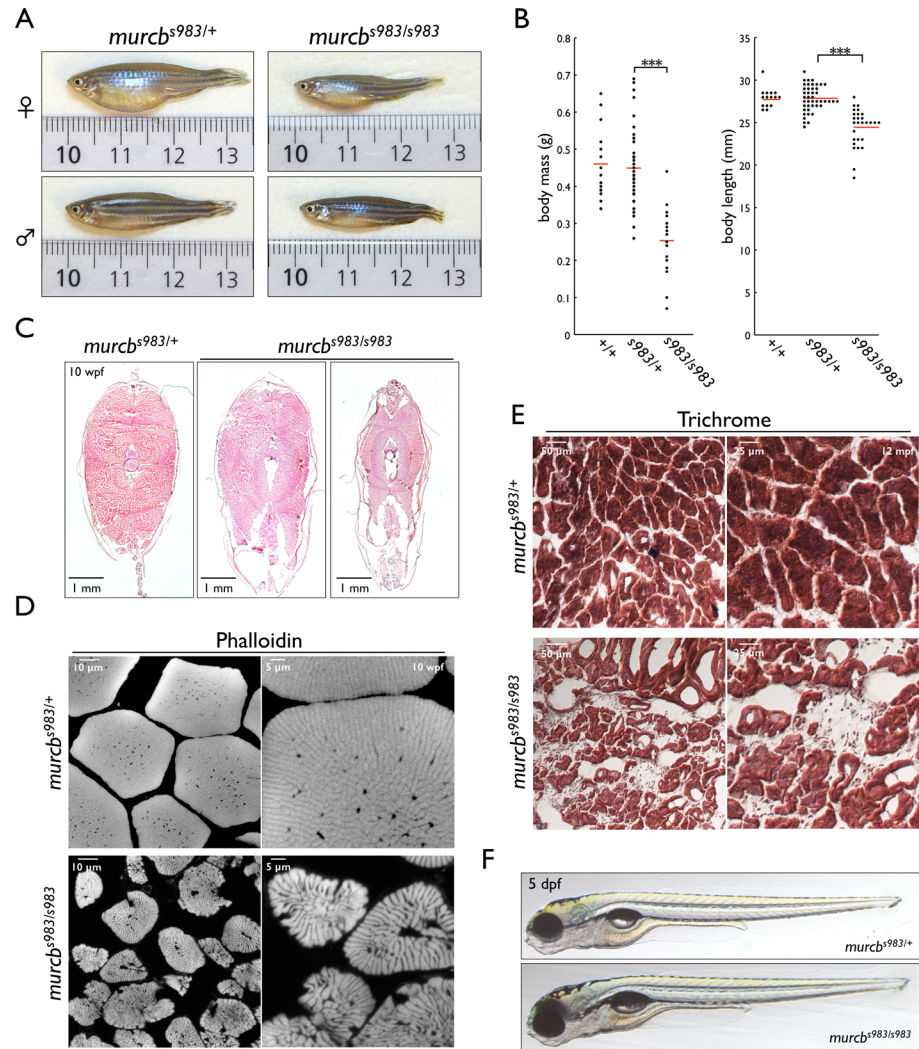


Fig 2. Characterization of Cavin4b/Murcb deficient zebrafish. A. Representative lateral views of *murcb*^{s983/s983} and *murcb*^{s983/+} sibling zebrafish at 10 wpf. Fish in the top panels are females while those in the bottom panels are males. B. Dot plots of body mass and length of 10 wpf wt, *murcb*^{s983/+}, and *murcb*^{s983/s983} zebrafish. Length measurements were made from the anterior point to the caudal fin/trunk boundary. Approximately equal numbers of male and female fish were used. The red line represents the mean. ***p<0.0005 C. H&E stain of 10 μm sections prepared from the trunk of 10 wpf *murcb*^{s983/+} and *murcb*^{s983/s983} zebrafish. Two examples of *murcb*^{s983/s983} fish of different sizes are shown. D. Phalloidin staining of 10 μm transverse sections prepared from the trunk of 10 wpf *murcb*^{s983/+} and *murcb*^{s983/s983} zebrafish. E. Trichrome staining of 10 μm transverse sections prepared from the trunk of 12 mpf *murcb*^{s983/+} and *murcb*^{s983/s983} zebrafish. F. Representative lateral views of *murcb*^{s983/+} and *murcb*^{s983/s983} zebrafish at 5 dpf.

doi:10.1371/journal.pgen.1006099.g002

0.891 m/s (Fig 4). Acceleration was also reduced in *murcb*^{s983/s983} fish at 14.2 m/s² compared with 26.1 m/s² for heterozygous siblings.

In order to determine whether there was a functional defect in Cavin4b/Murcb deficient skeletal muscle during development, we measured the maximum velocity and acceleration at 60 and 80 hpf. We found that at 60 hpf, mean maximum swimming velocity was not significantly different between *murcb*^{s983/+} and *murcb*^{s983/s983} embryos (Fig 4, 0.062 versus 0.056 m/s, respectively); however, mean maximum acceleration was reduced in *murcb*^{s983/s983} embryos (1.9 m/s²) compared to heterozygous siblings (2.6 m/s²). At 80 hpf, the difference in maximum velocity between *murcb*^{s983/+} and *murcb*^{s983/s983} larvae was significantly different (0.104 versus

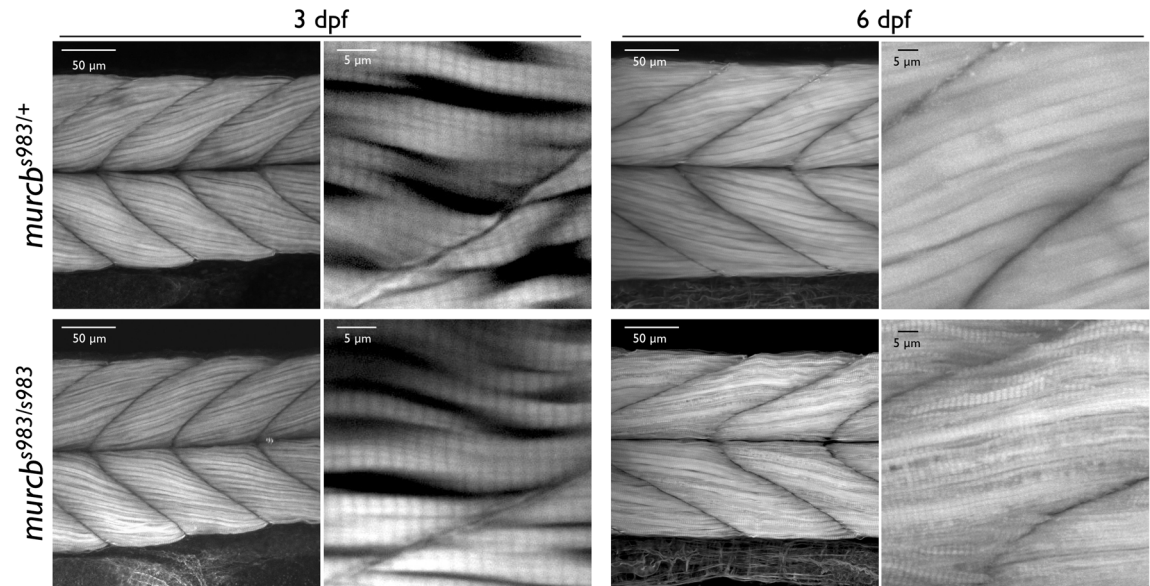


Fig 3. Filamentous actin analysis of Cavin4b/Murcb deficient zebrafish. Representative lateral views of confocal projections of phalloidin stained *murcb*^{s983/+} and *murcb*^{s983/s983} zebrafish at 3 dpf and 6 dpf. Skeletal muscle fibers are smaller and less consistent in size in *murcb* mutant animals compared to wild-type siblings.

doi:10.1371/journal.pgen.1006099.g003

0.077 m/s, respectively). The difference in maximum acceleration between *murcb*^{s983/+} and *murcb*^{s983/s983} larvae was also significantly different (3.69 versus 2.59 m/s², respectively). To rule out an effect of loss of Cavin4b/Murcb on the neuromuscular junctions, we performed whole mount α -bungarotoxin and Synaptic Vesicle glycoprotein 2 staining at 80 hpf. No obvious differences in post-synaptic structures could be observed between *murcb*^{s983/+} and *murcb*^{s983/s983} larvae (S4 Fig).

Dysregulation in voltage-gated ion channel mRNA expression and T-tubule defects in Cavin4b/Murcb deficient zebrafish

To investigate the underlying cause of the swimming defect in Cavin4b/Murcb deficient larvae, we isolated mRNA from mutant and sibling zebrafish at 72 hpf for microarray analysis. We examined the list of genes with an expression ratio of greater than 1.5 or less than 0.7 in *murcb*^{s983/s983} compared to *murcb*^{s983/+} samples by the PANTHER database protein class statistical overrepresentation test. 1309 transcripts were differentially expressed and recognized in the PANTHER database. Of these 55 are annotated in the ion channel protein class and 26 are annotated as voltage-gated ion channels while the expected number from 1309 input transcripts is 27 ($p = 0.000177$) and 10 ($p = 0.00291$), respectively (Fig 5). The relative mRNA expression levels of the differentially expressed genes in the voltage-gated ion channel class are also shown (Fig 5).

Because voltage-gated ion channels are critical to excitation-contraction coupling, we assessed the ultrastructure of the skeletal muscle in *murcb* mutant larvae to determine whether there were T-tubule abnormalities. Electron microscopy (EM) performed on 80 hpf larvae revealed that Cavin4b/Murcb deficiency was associated with a disruption of T-tubule development and maturation (Fig 6A). Quantification of the electron micrograph data showed that sibling controls had 88.3% intact T-tubule triad structures while Cavin4b/Murcb deficient larvae had 10% intact triads (S2 Table). Additionally, we found an increased number of caveolae in *murcb*^{s983/s983} larvae at 80 hpf compared with sibling controls (Fig 6B).

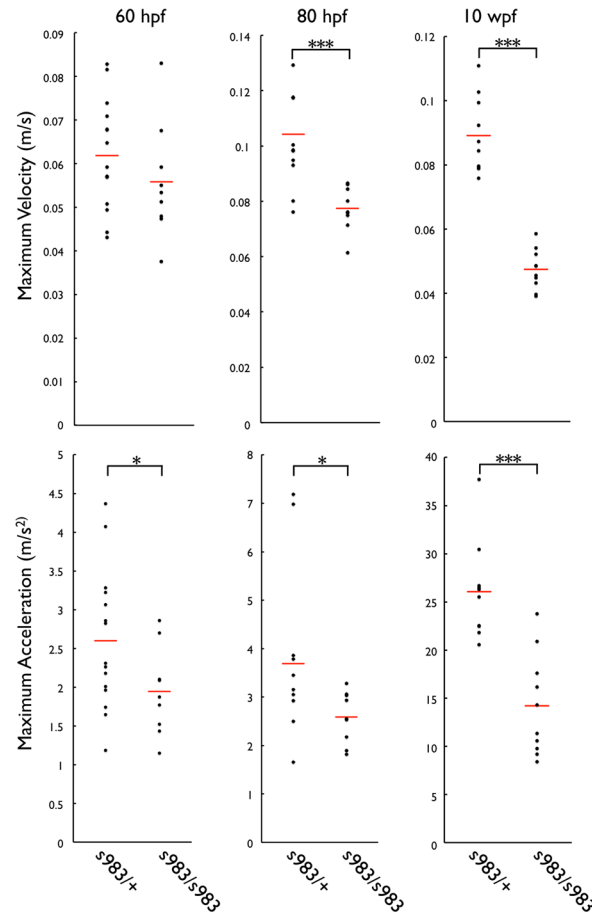


Fig 4. Swimming analysis of Cavin4b/Murcb deficient zebrafish. Dot plots of maximum swimming velocity and acceleration following the startle response of 60 hpf, 80 hpf, and 10 wpf *murcb*^{s983/+} and *murcb*^{s983/s983} zebrafish. The red line represents the mean. *p<0.05 ***p<0.0005

doi:10.1371/journal.pgen.1006099.g004

Cavin4b/Murcb is required for the localization of Caveolin proteins and Erk signaling *in vivo*

Because of the role of Cavin4/Murcb in the localization of Caveolin proteins, we examined the localization of Cav1 in transverse sections from 10 wpf fish and found increased and mislocalized anti-Cav1 immunoreactivity (Fig 7A). In sections from heterozygous siblings, Cav1 was predominantly localized to the surface of skeletal muscle fibers while in *murcb*^{s983/s983} skeletal muscle, there appeared to be additional Cav1 staining in the internal, putative membrane structures. In contrast to what has been reported in mammals [21,29], we found that Cav3 does not localize to the surface of skeletal muscle fibers in 10 wpf zebrafish, but rather appears to be associated with internal structures and not with Cavin4/Murcb (S5 Fig). Interestingly, Cavin4b/Murcb is nonetheless required for Cav3 localization, which is disrupted in *murcb*^{s983/s983} samples (Fig 7A).

In order to determine if Murcb has an effect on Cav1 localization in larvae, we performed whole mount antibody staining on larvae at 80 hpf. We found that Cav1 localization was altered in *murcb*^{s983/s983} larvae compared with heterozygous siblings with increased localization in a striated pattern (Fig 7B). To profile the staining of the striations, we measured the pixel density relative to the background of confocal images along a 3 μm distance perpendicular to

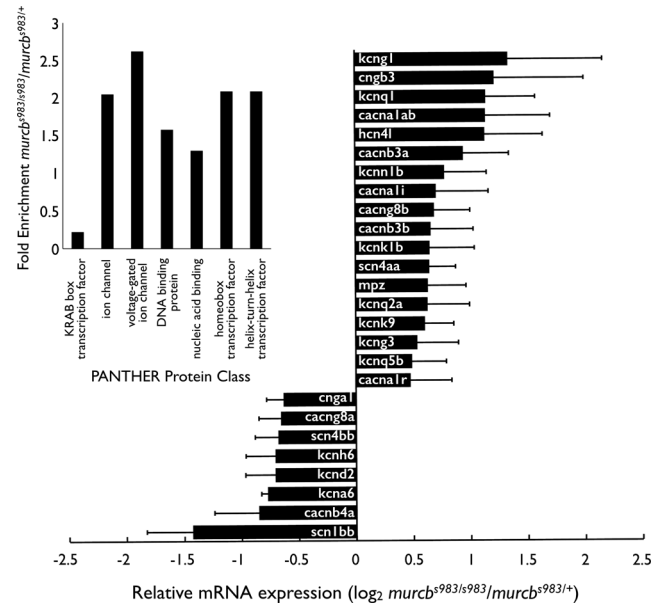


Fig 5. Transcriptional profiling of Cavin4b/Murcb deficient zebrafish. Inset: PANTHER Database protein class statistical overrepresentation test on microarray mRNA expression profiling from *murcb*^{s983/s983} compared to *murcb*^{s983/+} 72 hpf larvae. 1309 genes with greater than 1.5 fold or less than 0.7 fold expression difference in Cavin4b/Murcb deficient larvae compared to their heterozygous siblings were recognized in the database with 25708 genes comprising the *Danio rerio* reference list. Protein classes shown had a *p* value <0.05. The log₂ ratio of *murcb*^{s983/s983}/*murcb*^{s983/+} normalized microarray values from genes in the voltage-gated ion channel PANTHER protein class show that 26 members of the voltage-gated ion channel class were misregulated where 10 would be expected. Error bars represent SEM.

doi:10.1371/journal.pgen.1006099.g005

the striations. We then plotted the pixel intensity on the y-axis versus the distance across the image on the x-axis and found that compared to heterozygous siblings, *murcb*^{s983/s983} larvae have a higher Cav1 antibody reactivity in these striations.

Because caveolae are known to regulate growth factor signaling, we also assayed phosphorylated Erk1/2 in Cavin4b/Murcb deficient fish. We performed immunoblotting of skeletal muscle lysates from 3 *murcb*^{s983/s983} zebrafish and 3 *murcb*^{s983/+} siblings at 10 wpf and found in each mutant that phospho-Erk1/2 was increased relative to total Erk1/2 (Fig 7C).

Discussion

Here, we have shown a requirement for Cavin4b/Murcb in the development and function of skeletal muscle. Additionally, we have shown that Cavin4b/Murcb is necessary *in vivo* for caveolae function, Caveolin-1 and -3 localization, and Erk signaling in skeletal muscle. Our analyses of a targeted *murcb* mutation reveal the importance of caveolae for the formation of T-tubules during myogenesis and suggest an additional etiology for muscular dystrophy.

The complex membrane structures necessary for skeletal muscle function, such as the T-tubule network, require specialized membrane microdomains and their associated proteins for formation and function. Disruption of these proteins can lead to human disease. The nature of the Cavin4b/Murcb dependent muscle pathology described here is likely due to defects in the formation of T-tubules as evidenced by immature triad structures at 80 hpf. Caveolae are known to be abundant in T-tubules during development [22]; Cav3 is required for T-tubule shape and organization, and Cav3 mutant mice exhibit similar myopathologies as patients with type 1C limb-girdle MD [23]. Skeletal muscle fibers lacking a functional T-tubule network

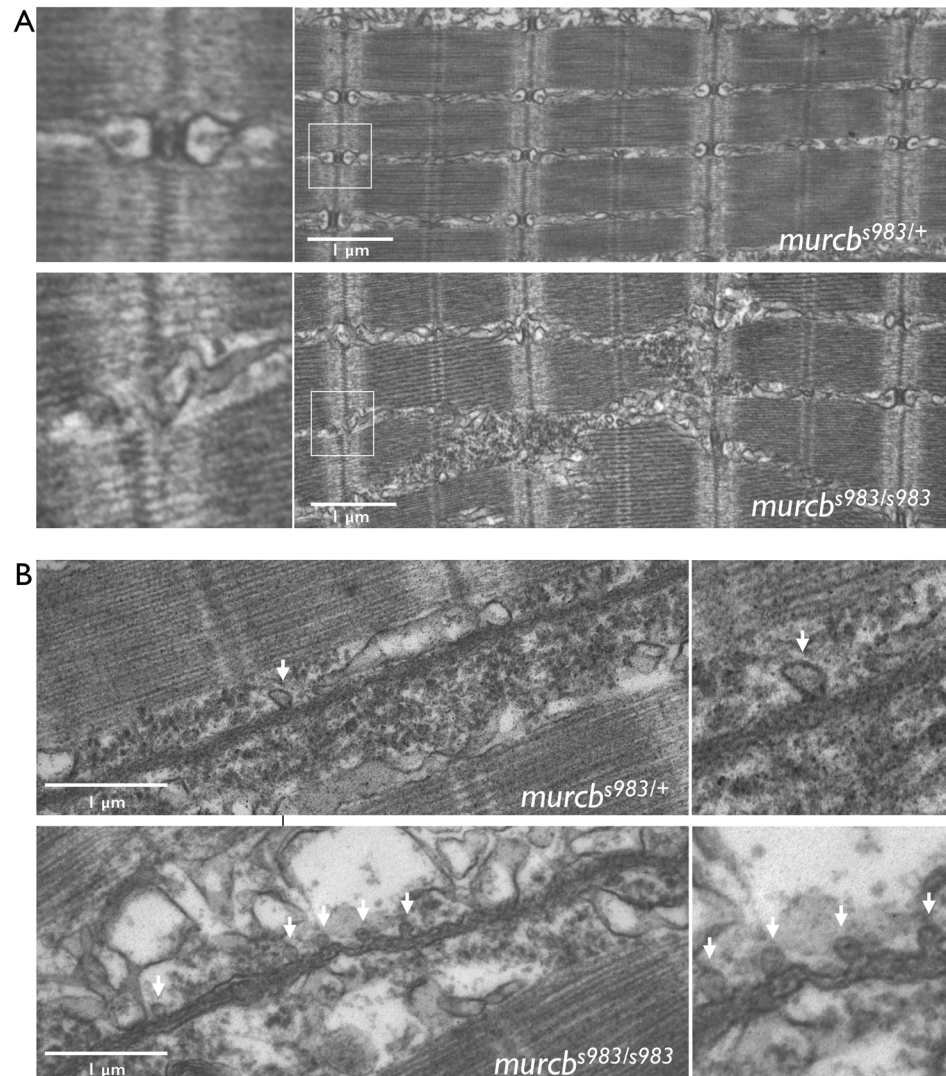


Fig 6. Ultra-structural analysis of Cavin4b/Murcb deficient skeletal muscle. A. Representative electron micrographs of *murcb*^{s983/+} and *murcb*^{s983/s983} zebrafish at 80 hpf. T-tubule triad structures are indicated with a box and enlargements of this region are shown on the left. B. Representative electron micrographs of *murcb*^{s983/+} and *murcb*^{s983/s983} zebrafish at 80 hpf. Caveolae are indicated by arrows. Enlargements from the micrographs are shown on the right.

doi:10.1371/journal.pgen.1006099.g006

likely have calcium flux and excitation-contraction coupling deficiencies that could result in ion channel gene expression changes initially, and subsequently result in muscle wasting [6].

Several genetic models have yielded insights into the pathology of other types of MD. For example ENU-induced mutations in zebrafish laminin $\beta 2$ (*lamb2/softy*) cause embryonic muscle degeneration due to loss of the extracellular matrix supporting the sarcolemma during skeletal muscle contraction [36]. Zebrafish *dystrophin* (*sap/dmd*) mutants display skeletal muscle fiber detachment and membrane damage resulting in uptake of Evans blue dye [37]. These models of MD present phenotypes early in development and are therefore identifiable in a forward genetic screen. In contrast *cavin4b/murcb*, a much smaller gene than *lamb2* or *dmd*, is less likely to be mutagenized by random means and is more likely to be determined to be phenotypically normal prior to 5 dpf. Therefore, a targeted genetic approach was critical to

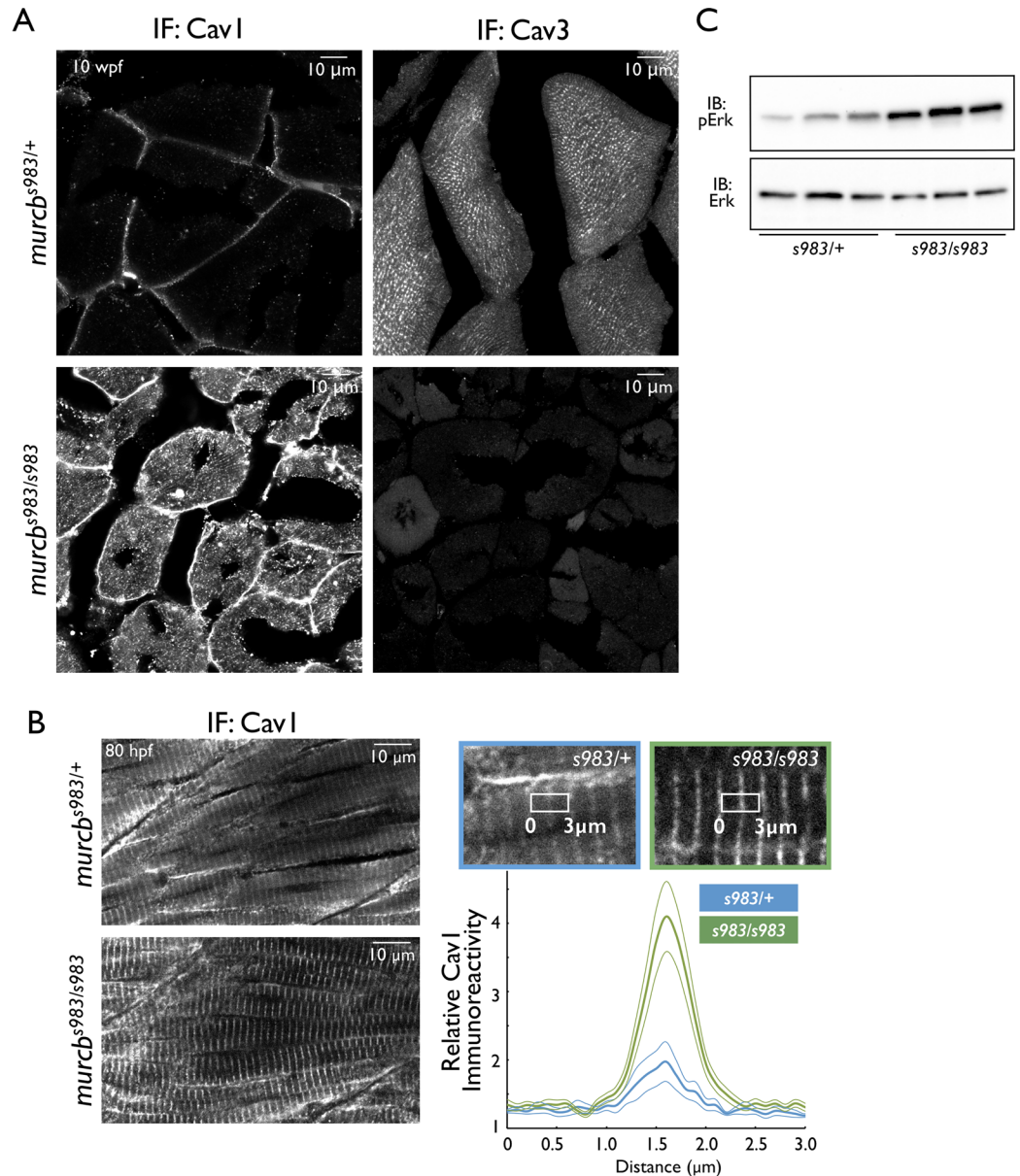


Fig 7. Caveolin expression and growth factor signaling in Cavin4b/Murcb deficient zebrafish. A. Representative confocal micrographs of Cav1 and Cav3 immunostaining of 10 μ m transverse sections prepared from the trunk of 10 wpf *murcb^{s983/+}* and *murcb^{s983/s983}* zebrafish. B. Representative confocal micrographs of Cav1 whole mount immunostaining in *murcb^{s983/+}* and *murcb^{s983/s983}* zebrafish at 80 hpf. Mean relative fluorescence profiles from at least 6 larvae for each genotype. Pixel intensity was measured across a 3 μ m segment covering a single striation and plotted relative to the background intensity between stria. SEM is represented by thin lines. C. Immunoblot of phospho-Thr202/Tyr204-Erk1/2 and total Erk1/2 from skeletal muscle prepared from 3 *murcb^{s983/+}* and 3 *murcb^{s983/s983}* 10 wpf zebrafish.

doi:10.1371/journal.pgen.1006099.g007

understand the function of *murcb* in zebrafish. The pathomechanics of Cavin4b/Murcb deficiency appear to be rather different than those of dystrophin deficiency as *dystrophin* mutant larvae show muscle detachment by 48 hpf and die around 31 dpf [37]. Therefore, *cavin4b/murcb* mutants represent a distinct tool to better understand processes such as T-tubulogenesis and how caveolinopathies lead to skeletal muscle diseases.

Mutations in other Cavin genes have been linked to skeletal muscle disease. Mutations in human CAVIN1 (PTRF) have been reported to cause MD and generalized lipodystrophy, defects that are likely secondary to caveolae disruption [38]. Patients in this study had histopathologies in common with MD such as variable skeletal muscle fiber size, while other phenotypic changes were not consistently present, suggesting the influence of genetic modifiers. It will be interesting to examine CAVIN4 localization and expression in patients with CAVIN1 mutations, as there appears to be interdependence in their expression and regulation. Indeed, it was recently shown that in *Cavin1* KO mice, CAV1 protein expression was reduced and CAVIN4 expression was not detectable [39]. This reduction in CAVIN4 expression was evident in both skeletal muscle and heart, and suggests that a homeostatic feedback mechanism exists that either stabilizes a Cavin hetero-oligomeric complex or regulates transactivation. Kovtun et al. have recently characterized Cavin interactions, finding that CAVIN1 can bind to other Cavin family members as well as homo-oligomerize [31]. This interaction is mediated through the Helical Region (HR1), which forms a trimeric coiled coil. Cavin oligomerization seems to be organ-specific [39], and may depend on interactions with CAVIN4 or CAV3, which have restricted expression patterns. In human skeletal muscle, CAVIN4 expression correlates very highly with mosaic expression of CAV3 [29].

While the function of Cavin4/Murc remains poorly understood, a role in signal transduction has emerged in recent studies. In cultured cardiomyocytes, hypoxia induces Cavin4/Murc expression in an Erk-dependent manner [40]. A Cavin4/Cav3 complex co-localizes with α 1-adrenergic receptors (α 1-AR) in cardiomyocytes and α 1-AR-induced cardiac hypertrophy is attenuated in *Cavin4/Murc* mutant mice [30].

Apart from a direct upstream effect of Cavin4/Murc on Erk signaling, one explanation for the observed increase in phosphorylated Erk in Cavin4/Murc deficient zebrafish skeletal muscle is chronic injury [41]. Satellite cell exhaustion from continual repair is thought to contribute to the pathology of MD. Interestingly, *Cavin4/Murc*, but not *Cav1* or *Cav3*, is highly upregulated in “alert” satellite cells [42] (see <http://www.ncbi.nlm.nih.gov/geo/query/acc.cgi?acc=GSE55490>) raising the possibility that Cavin proteins are necessary for muscle membrane structures as well as for repair, perhaps through a role in cell fusion [43,44]. Further examination of the Cavin4/Murc KO mouse, which in contrast to zebrafish has not been reported to have a skeletal muscle phenotype [30], should be directed toward muscle injury and repair.

Caveolar proteins have been linked to cardiomyopathies as well as MD [45–47]. In mouse, mutations in *Cav3* result in cardiomyopathy characterized by myocyte hypertrophy, dilation of the heart chambers, and a reduction in fractional shortening [48]. Given the interdependence between Cavin and Caveolin protein expression and distribution, the role of Cavin4 in cardiomyopathy should be studied further. CAVIN4 mutations have previously been linked to Dilated Cardiomyopathy (DCM). Rodriguez et al found 6 heterozygous mutations (N128K, R140W, L153P, S307T, P324L, and S364L) in patients with DCM but none in patients with hypertrophic cardiomyopathy or in healthy controls [49]. Our Cavin4b/Murcb deficient fish line will be a useful tool to determine whether these mutations in human CAVIN4 indeed result in a loss of protein function. As there is an overexpression phenotype for Cavin4/Murc reported in mouse [30], the cloning of the zebrafish *cavin4b/murcb* promoter/enhancer will likely be necessary for rescue experiments with the human mutant alleles.

The pathomechanics of the various forms of MD have been of great interest due to the severity of the disease, limited treatment options, and the difficulty of implementing gene therapy [4]. Due to the accessibility of developing skeletal muscle in zebrafish larvae, zebrafish models of MD can be used to test how aberrant calcium flux, T-tubule development, and growth factor signaling can impact progressive skeletal muscle disease. A targeted mutation approach has revealed that Cavin4b/Murcb is necessary for the development of the T-tubule

network during embryonic myogenesis and the proper localization of Caveolin-1 and -3 in adult muscle. These changes are associated with reduced skeletal muscle fiber size and uniformity, fibrosis, and reduced muscle function, suggesting that CAVIN4 may be important to the etiology of MD early in the development of skeletal muscle.

Materials and Methods

Immunoblotting, immunostaining, histology and cell death visualization

Antibodies used for immunoblotting were against Erk1/2 (Cell Signaling, 9102), phosphoThr202/Tyr204-Erk1/2 (Cell Signaling, 4370), Caveolin-1 (BD Transduction Labs, 610059), Caveolin-3 (BD Transduction Labs, 610420), and Cavin4/Murc (Sigma-Aldrich, HPA021021). Whole mount antibody and phalloidin stainings were performed on larvae fixed with 4% paraformaldehyde, 4% sucrose, 77 mM Na₂HPO₄, 22.6 mM NaH₂PO₄, 120 μM CaCl₂ pH 7.35 overnight at 4°C, permeabilized with PBS, 0.5% Triton X-100 for 3 hours at room temperature, and stained with Alexa-488 conjugated phalloidin (Cytoskeleton, PHDG1) at a 1:100 dilution in PBS, 0.5% Triton X-100. Whole mount immunofluorescence staining was performed on fixed larvae that were dehydrated in 4 steps to 70% ethanol in PBS and stored at 4°C. Prior to staining, larvae were rehydrated in 4 steps to 1X PBS, digested with proteinase K at 30 μg/ml for 30 minutes at room temperature and blocked with PBS, 5% normal goat serum (NGS), 0.5% Triton X-100 and incubated with indicated antibodies diluted 1:100 in PBS, 5% NGS, 0.5% Triton X-100 overnight at 4°C. Larvae were then washed 4 times with PBS with 0.5% Triton X-100, incubated with secondary antibodies, mounted in agarose, and imaged on an LSM700 confocal microscope (Zeiss). H&E and immunofluorescence stainings were performed on trunk tissue dissected from adult fish and fixed in 4% paraformaldehyde, 4% sucrose, 77 mM Na₂HPO₄, 22.6 mM NaH₂PO₄, 120 μM CaCl₂ pH 7.35 overnight at 4°C, transferred to PBS with 20% sucrose for 24 hours and then frozen in OCT for cryosectioning. 10 μm transverse cryosections were stored at -80°C prior to staining. Sections were briefly dried, then permeabilized with PBS with 0.5% Triton X-100. Alexa-488 conjugated phalloidin was diluted 1:100 in PBS with 0.5% Triton X-100 and incubated for 3 hours at room temperature followed by 5 washes with PBS with 0.5% Triton X-100. Indicated antibodies were diluted in PBS, 5% NGS, 0.5% Triton X-100 and incubated overnight at 4°C. Sections were then washed 4 times with PBS with 0.5% Triton X-100 and incubated with Alexa-488 or Alexa-568 conjugated secondary antibodies and imaged on an LSM700 confocal microscope. Presynaptic structures were visualized in 80 hpf fish that were fixed in 4% paraformaldehyde for 4 hours at 4°C, washed 4 times with PBS, and permeabilized with protease K (10 μg/ml) for 30 minutes at room temperature. Larvae were then washed in PBS, 0.5% Triton X-100, 1% DMSO (PBT-DMSO) before blocking overnight at 4°C in PBT-DMSO with 1% BSA and 2% goat serum. Antibodies against Synaptic Vesicle 2 (SV2, Developmental Studies Hybridoma Bank) were diluted 1:20 in blocking solution and incubated overnight at 4°C. After washing with PBT-DMSO, larvae were incubated with Alexa-568 conjugated donkey anti-mouse antibodies (Molecular Probes) for 2 hours at room temperature. Larvae were then washed, mounted, and imaged on an LSM 780 confocal microscope (Zeiss). Postsynaptic structures were visualized in 80 hpf fish that were fixed in 4% paraformaldehyde for 4 hours at 4°C, washed 4 times with PBS, permeabilized with 0.2% collagenase P (Roche, 11213805001) for 50 minutes then washed 4 times with PBS. Embryos and larvae were incubated with 20 μg/ml Tetramethylrhodamine (TRITC) conjugated bungarotoxin (Sigma Aldrich, T0195) for 30 min at room temperature. Larvae were then washed, mounted, and imaged on an LSM 780 confocal microscope. Acridine orange (Sigma, 235474) staining was used to identify apoptosis in live larvae at 80 hpf. Larvae were incubated in a solution of 10 μg/ml acridine orange for 30 minutes, then washed with PBS

three times and imaged through a Fluorescein-Isothiocyanate (FITC) filter using an LSM780 confocal microscope.

Mass spectrometry

Sample preparation. 3 dpf zebrafish larvae were genotyped and trunk tissue was homogenized in SDS lysis buffer (4% SDS in 100 mM Tris/HCl pH 7.6). For complete cell lysis, samples were heated at 95°C for 10 minutes. The homogenate was spun at 16,000 g for ten minutes and protein concentration was estimated using the DC protein assay (Biorad). Lysates were precipitated for one hour using 4 volumes of ice-cold acetone. The protein pellet was dissolved in 6 M urea, 2 M thiourea, 10 mM HEPES, pH 8 and subjected to digestion in solution. Next, protein disulfide bonds were reduced with 10 mM dithiothreitol (DTT) and alkylated with 55 mM iodoacetamide. In-solution digestion was done with Lys-C (Wako) (protein to Lys-C ratio = 100:1) overnight at room temperature. The resulting peptide mixtures were concentrated and desalted using the Stop and Go Extraction (STAGE) technique [50].

Liquid Chromatography and Mass Spectrometry: A binary buffer system consisting of buffer A (0.1% formic acid or 0.5% acetic acid) and buffer B (80% Acetonitrile, 0.1% formic acid or 0.5% acetic acid) was used for peptide separation on an Easy nano-flow UHPLC system (Thermo Fisher Scientific, Odense Denmark). This system was coupled via a nano electrospray ionization source to the QExactive mass spectrometer. Peptide elution from the in-house packed 50 cm columns (1.8 μ m Beads, 75 μ m ID, Dr. Maisch, Germany) was achieved by increasing the relative amount of B from 7% to 38% in a linear shape within 240 min at a column temperature of 45°C, followed by 5 min at 95% B and gradients were completed by a re-equilibration time of 5 min to 5% B. Acquisition of MS spectra in a mass range of 350–1650 m/z was done using an AGC target of 3E6 at a resolution of 70000 (200 m/z). The instrument worked in a data dependent mode, isolation of the ten most intense peaks for HCD fragmentation (25 collision energy) in a 100–1650 m/z mass range. The AGC target was set to 5E5 combined with a resolution of 35000 at 200 m/z, while a maximum injection time of 60 ms was used.

Data analysis. Complete set of raw files was processed using MaxQuant (1.5.2.8) and the implemented Andromeda search engine. For protein assignment ESI-MS/MS fragmentation spectra were correlated to the Uniprot zebrafish database (*Danio rerio*, 40368 entries) including a list of contaminants. A maximum of two missed cleavages and a mass tolerance of 4.5 ppm and 7 ppm for MS/MS first and main search were set, respectively. Carbamidomethyl at cysteine residues was defined as a fixed modification and oxidation at methionine and acetylation at the N-terminus of proteins were set as variable modifications. A minimal peptide length of 7 amino acids after Lys-C specificity for protein assignment and for quantification a minimal ratio count of 2 was required. Further, only unique peptides were used for quantification and the FDR was controlled by the revert algorithm in MaxQuant at the peptide and protein level. Data visualization was performed using the statistical environment R and MaxQuant output text files were filtered for contaminants and reverse entries. Gene Ontology annotation based on Uniprot identifiers was carried out in the Perseus software (Max Planck Institute, Martinsried).

Membrane integrity assay

Evans Blue Dye (Sigma Aldrich, E2129) was dissolved in egg water at 0.1% (w/v). 4 dpf 1-phenyl-2-thiourea (PTU)-treated larvae were transferred to a nylon mesh basket and submerged in dye for 60 minutes. The basket was removed from the dye solution, washed with egg water, and larvae were transferred to a fresh dish for imaging and genotyping.

Microarray and PANTHER analysis

RNA and gDNA were extracted from individual larvae at 72 hpf using Trizol (Life Technologies). Following genotyping, the aqueous phases from at least 10 Trizol extractions were combined by genotype and purified over microspin columns (ZymoResearch). RNA expression from heterozygous and mutant larvae was analyzed by single-color microarray (8x60K Zebrafish Array XS, Oaklabs, Germany). The arrays were imaged using a SureScan Microarray Scanner and Agilent's Feature Extraction software version 11 was used to read and process the TIFF images. Data were normalized by using the ranked median quantiles [51]. Microarray data were archived in the NCBI database (GSE70858).

PANTHER (v 9.0, release 20140124) database protein class statistical overrepresentation test (release 20141219, with Bonferroni correction) was performed on a list of genes that expressed at a ratio of greater than or equal to 1.5 times or less than or equal to 0.7 times the expression found in heterozygous *murcb* versus homozygous *murcb* larvae and having a normalized signal with a value greater than 50. 1309 differentially expressed genes were identified in the database. 25708 genes comprise the reference set for *Danio rerio*.

Swimming analysis

Swimming speed and acceleration were measured in 10-week-old fish that were transferred to a 40 cm by 40 cm tray containing system water above which a digital camera was mounted. Movies were recorded following the startle response and frame-by-frame location within the tray over time was determined using PhysMo V2 software (<http://physmo.sf.net>). Distance calibration was made using a ruler submerged in the tray. Measurements of swimming larvae were performed in a similar manner in a 10 cm dish. Deformed fish were not used in the swimming analysis. Statistical significance was determined using a two-tailed unequal variance *t*-test.

TALEN mutagenesis, genotyping and RT-PCR

TALENs were designed against *murcb* using the TALEN Targeter 2.0 software [33,34]. The plasmid kit used for generation of TALENs was a gift from Daniel Voytas and Adam Bogdanove (Addgene kit # 1000000024). Capped mRNA encoding the TALEN was generated using the mMACHINE SP6 Transcription Kit (Life Technologies, AM1340) and 200 pg of each arm were injected into one-cell stage embryos. TALENs were tested by HRMA analysis on an amplicon from gDNA harvested from individual embryos at 24 hpf. Injected F0 siblings from functional TALENs were raised to adulthood and outcrossed to identify founders. F1 fish were then raised to adulthood and gDNA was isolated from the caudal fin to identify F1 heterozygous fish by HRMA. PCR products from the HRMA were cloned into pGEM-T Easy (Promega) for sequencing. gDNA was isolated by digesting individual embryos or clipped fins in proteinase K at 65°C for 1 hour with occasional vortexing followed by inactivation at 95°C for 10 minutes. For screening of founders, HRMA primers were designed to amplify between 80 and 100 nucleotides. Upon identification of a suitable allele, HRMA primers were redesigned to amplify a region immediately surrounding the mutation (Forward: 5'-TCTCTGCTGGAGAGGGTGTC, Reverse: 5'-CTGGCAGGCTGAACATTGT, Annealing temperature: 65°C). RT-PCR primers for *murca* were: Forward: 5'-TGTGATCTATCAGGGTGAAAAG, Reverse: 5'-TGGAGAACGCAGCCTTGATGTTTC. RT-PCR primers for *murcb* were: Forward: 5'-GTCATCTACCAGGGAGATAATGAG, Reverse: 5'-GTCATGTTCTCGCGTGAGAAGGTC.

Transmission electron microscopy

Zebrafish larvae were fixed with 3% glutaraldehyde (Merck), followed by 4% OsO₄ in 0.1 mmol/L sodium cacodylate buffer (pH 7.4). After dehydration in ethanol and propylene oxide, they were embedded in Epon as described. Semi-thin (1 μm) sections were stained with toluidine blue and viewed in a Leica DM microscope. Ultrathin sections were stained with uranyl acetate and lead citrate and viewed and photographically recorded under a Philips CM 10 electron microscope.

Ethics statement

Animal studies were carried out following guidelines and standard procedures set forth by the Regierungspräsidium Gießen Dezernat V 54 (Protocol No. B2/342).

Supporting Information

S1 Fig. Murc conservation and expression in zebrafish. A. Protein alignment of zebrafish Murca and Murcb with human, mouse, rat, cow, and *Xenopus* orthologs. B. Zebrafish *murc* genes share a similar intron-exon structure with human *MURC* having two exons and a single intron. White boxes represent UTRs. C. Phylogenetic analysis of zebrafish Murca and Murcb. D. Whole mount *in situ* hybridization of *murca* mRNA in zebrafish embryos at 48 hpf. Top: lateral view. Bottom left: magnified lateral view. Bottom right: magnified dorsal view. (TIFF)

S2 Fig. Mass Spectrometry of lysates generated from a pool of genotyped larval trunk tissue. A. Total ion chromatogram of an in-solution digest from *murcb*^{s983/+} and *murcb*^{s983/s983} larvae. Arrow at 72.64 minutes retention time points to the peptide mass of 631.35 m/z (see arrow in B). B. MS spectra from *murcb*^{s983/+} and *murcb*^{s983/s983} samples. (TIFF)

S3 Fig. Analysis of Cavin4b/Murcb deficient zebrafish. A. Evans blue dye assay of membrane integrity. The top panel is an injured somite and is shown as a positive control. No significant changes were observed between mutants and heterozygous controls. B. Representative maximal projection confocal images from live whole mount acridine orange staining of *murcb*^{s983/+} and *murcb*^{s983/s983} zebrafish trunk at 80 hpf. Arrows point to DNA fragmentation. Dotted lines outline the larvae. No significant changes were observed between mutants and heterozygous controls. C. RT-PCR analysis of *murca* and *murcb* mRNA from *murcb*^{s983/+} and *murcb*^{s983/s983} larvae at 72 hpf. No significant changes were observed between mutants and heterozygous controls. (TIFF)

S4 Fig. Neuromuscular junction analysis of Cavin4b/Murcb deficient zebrafish. Representative confocal maximal projections of whole mount Synaptic Vesicle glycoprotein 2 (SV2, left) and α-bungarotoxin (α-BTX, right) staining of the trunk of 80 hpf *murcb*^{s983/+} and *murcb*^{s983/s983} zebrafish. SV2 immunofluorescence was used to visualize presynaptic structures; α-BTX staining was used to visualize postsynaptic structures. Synaptic punctae per somite were quantified using ImageJ (dotplot, bottom). (TIFF)

S5 Fig. Immunofluorescence localization of Cav3 and Murc in adult skeletal muscle. Confocal micrographs of transverse sections prepared from 10 wpf *murcb*^{s983/+} zebrafish and stained with anti-Murc (red) and anti-Cav3 (green). Merged views are shown on the right and below. (TIFF)

S1 Table. Label-free quantification (LFQ) of peptides from Murcb deficient larvae and sibling controls.

(DOCX)

S2 Table. Quantification of intact triads from electron micrographs of Cavin4b/Murcb deficient and sibling zebrafish larvae.

(DOCX)

Acknowledgments

We thank Ana Ayala, Milagritos Alva, and Mark Sklar for zebrafish husbandry at UCSF, and Rita Retzlöff and her team for zebrafish husbandry at the MPI Bad Nauheim. We also thank Carol Yang and Michelle Collins for critical reading of the manuscript.

Author Contributions

Conceived and designed the experiments: MPH BN FR OAS SH MK SK. Performed the experiments: MPH BN FR OAS SH MK SK. Analyzed the data: MPH BN FR SH MK SK. Wrote the paper: MPH OAS DYRS. Supervised the research: DYRS.

References

1. Emery AE. The muscular dystrophies. *The Lancet*. 2002; 359: 687–695. doi: [10.1016/S0140-6736\(02\)07815-7](https://doi.org/10.1016/S0140-6736(02)07815-7)
2. Brooke MH, Fenichel GM, Griggs RC, Mendell JR, Moxley R, Florence J, et al. Duchenne muscular dystrophy Patterns of clinical progression and effects of supportive therapy. *Neurology*. 1989; 39: 475–475. doi: [10.1212/WNL.39.4.475](https://doi.org/10.1212/WNL.39.4.475) PMID: [2927672](https://pubmed.ncbi.nlm.nih.gov/2927672/)
3. Jefferies JL, Eidem BW, Belmont JW, Craigen WJ, Ware SM, Fernbach SD, et al. Genetic Predictors and Remodeling of Dilated Cardiomyopathy in Muscular Dystrophy. *Circulation*. 2005; 112: 2799–2804. doi: [10.1161/CIRCULATIONAHA.104.528281](https://doi.org/10.1161/CIRCULATIONAHA.104.528281) PMID: [16246949](https://pubmed.ncbi.nlm.nih.gov/16246949/)
4. Shin J, Tajrishi MM, Ogura Y, Kumar A. Wasting mechanisms in muscular dystrophy. *Int J Biochem Cell Biol*. 2013; 45: 2266–2279. doi: [10.1016/j.biocel.2013.05.001](https://doi.org/10.1016/j.biocel.2013.05.001) PMID: [23669245](https://pubmed.ncbi.nlm.nih.gov/23669245/)
5. Deconinck N, Dan B. Pathophysiology of Duchenne Muscular Dystrophy: Current Hypotheses. *Pediatr Neurol*. 2007; 36: 1–7. doi: [10.1016/j.pediatrneurol.2006.09.016](https://doi.org/10.1016/j.pediatrneurol.2006.09.016) PMID: [17162189](https://pubmed.ncbi.nlm.nih.gov/17162189/)
6. Ohlendieck K. The Pathophysiological Role of Impaired Calcium Handling in Muscular Dystrophy. 2000; Available: <http://www.ncbi.nlm.nih.gov/books/NBK6173/>
7. Millay DP, Goonasekera SA, Sargent MA, Maillet M, Aronow BJ, Molkentin JD. Calcium influx is sufficient to induce muscular dystrophy through a TRPC-dependent mechanism. *Proc Natl Acad Sci*. 2009; 106: 19023–19028. doi: [10.1073/pnas.0906591106](https://doi.org/10.1073/pnas.0906591106) PMID: [19864620](https://pubmed.ncbi.nlm.nih.gov/19864620/)
8. Bradley WG, Fulthorpe JJ. Studies of sarcolemmal integrity in myopathic muscle. *Neurology*. 1978; 28: 670–677. PMID: [79157](https://pubmed.ncbi.nlm.nih.gov/79157/)
9. Matsuda R, Nishikawa A, Tanaka H. Visualization of Dystrophic Muscle Fibers in Mdx Mouse by Vital Staining with Evans Blue: Evidence of Apoptosis in Dystrophin-Deficient Muscle. *J Biochem (Tokyo)*. 1995; 118: 959–963. doi: [10.1093/jb/118.5.959](https://doi.org/10.1093/jb/118.5.959)
10. Pardo JV, Siliciano JD, Craig SW. A vinculin-containing cortical lattice in skeletal muscle: transverse lattice elements (“costameres”) mark sites of attachment between myofibrils and sarcolemma. *Proc Natl Acad Sci U S A*. 1983; 80: 1008–1012. PMID: [6405378](https://pubmed.ncbi.nlm.nih.gov/6405378/)
11. Campbell KP. Three muscular dystrophies: Loss of cytoskeleton-extracellular matrix linkage. *Cell*. 1995; 80: 675–679. doi: [10.1016/0092-8674\(95\)90344-5](https://doi.org/10.1016/0092-8674(95)90344-5) PMID: [7889563](https://pubmed.ncbi.nlm.nih.gov/7889563/)
12. Rybakova IN, Patel JR, Ervasti JM. The Dystrophin Complex Forms a Mechanically Strong Link between the Sarcolemma and Costameric Actin. *J Cell Biol*. 2000; 150: 1209–1214. doi: [10.1083/jcb.150.5.1209](https://doi.org/10.1083/jcb.150.5.1209) PMID: [10974007](https://pubmed.ncbi.nlm.nih.gov/10974007/)
13. Lapidos KA, Kakkar R, McNally EM. The Dystrophin Glycoprotein Complex Signaling Strength and Integrity for the Sarcolemma. *Circ Res*. 2004; 94: 1023–1031. doi: [10.1161/01.RES.0000126574.61061.25](https://doi.org/10.1161/01.RES.0000126574.61061.25) PMID: [15117830](https://pubmed.ncbi.nlm.nih.gov/15117830/)
14. Hopkins PM. Skeletal muscle physiology. *Contin Educ Anaesth Crit Care Pain*. 2006; 6: 1–6. doi: [10.1093/bjaceaccp/mki062](https://doi.org/10.1093/bjaceaccp/mki062)

15. Al-Qusairi L, Laporte J. T-tubule biogenesis and triad formation in skeletal muscle and implication in human diseases. *Skelet Muscle*. 2011; 1: 26. doi: [10.1186/2044-5040-1-26](https://doi.org/10.1186/2044-5040-1-26) PMID: [21797990](https://pubmed.ncbi.nlm.nih.gov/21797990/)
16. Bassel-Duby R, Olson EN. Signaling Pathways in Skeletal Muscle Remodeling. *Annu Rev Biochem*. 2006; 75: 19–37. doi: [10.1146/annurev.biochem.75.103004.142622](https://doi.org/10.1146/annurev.biochem.75.103004.142622) PMID: [16756483](https://pubmed.ncbi.nlm.nih.gov/16756483/)
17. Waugh TA, Horstick E, Hur J, Jackson SW, Davidson AE, Li X, et al. Fluoxetine prevents dystrophic changes in a zebrafish model of Duchenne muscular dystrophy. *Hum Mol Genet*. 2014; 23: 4651–4662. doi: [10.1093/hmg/ddu185](https://doi.org/10.1093/hmg/ddu185) PMID: [24760771](https://pubmed.ncbi.nlm.nih.gov/24760771/)
18. Al-Qusairi L, Weiss N, Toussaint A, Berbey C, Messaddeq N, Kretz C, et al. T-tubule disorganization and defective excitation-contraction coupling in muscle fibers lacking myotubularin lipid phosphatase. *Proc Natl Acad Sci*. 2009; 106: 18763–18768. doi: [10.1073/pnas.0900705106](https://doi.org/10.1073/pnas.0900705106) PMID: [19846786](https://pubmed.ncbi.nlm.nih.gov/19846786/)
19. Lee E, Marcucci M, Daniell L, Pypaert M, Weisz OA, Ochoa G-C, et al. Amphiphysin 2 (Bin1) and T-Tubule Biogenesis in Muscle. *Science*. 2002; 297: 1193–1196. doi: [10.1126/science.1071362](https://doi.org/10.1126/science.1071362) PMID: [12183633](https://pubmed.ncbi.nlm.nih.gov/12183633/)
20. Gazzero E, Sotgia F, Bruno C, Lisanti MP, Minetti C. Caveolinopathies: from the biology of caveolin-3 to human diseases. *Eur J Hum Genet*. 2009; 18: 137–145. doi: [10.1038/ejhg.2009.103](https://doi.org/10.1038/ejhg.2009.103) PMID: [19584897](https://pubmed.ncbi.nlm.nih.gov/19584897/)
21. Galbati F, Engelman JA, Volonte D, Zhang XL, Minetti C, Li M, et al. Caveolin-3 Null Mice Show a Loss of Caveolae, Changes in the Microdomain Distribution of the Dystrophin-Glycoprotein Complex, and T-tubule Abnormalities. *J Biol Chem*. 2001; 276: 21425–21433. doi: [10.1074/jbc.M100828200](https://doi.org/10.1074/jbc.M100828200) PMID: [11259414](https://pubmed.ncbi.nlm.nih.gov/11259414/)
22. Parton RG, Way M, Zorzi N, Stang E. Caveolin-3 Associates with Developing T-tubules during Muscle Differentiation. *J Cell Biol*. 1997; 136: 137–154. doi: [10.1083/jcb.136.1.137](https://doi.org/10.1083/jcb.136.1.137) PMID: [9008709](https://pubmed.ncbi.nlm.nih.gov/9008709/)
23. Galbati F, Volonté D, Engelman JA, Scherer PE, Lisanti MP. Targeted Down-regulation of Caveolin-3 Is Sufficient to Inhibit Myotube Formation in Differentiating C2C12 Myoblasts Transient Activation of p38 Mitogen-Activated Kinase Is Required For Induction of Caveolin-3 Expression And Subsequent Myotube Formation. *J Biol Chem*. 1999; 274: 30315–30321. doi: [10.1074/jbc.274.42.30315](https://doi.org/10.1074/jbc.274.42.30315) PMID: [10514527](https://pubmed.ncbi.nlm.nih.gov/10514527/)
24. Nixon SJ, Wegner J, Ferguson C, Méry P-F, Hancock JF, Currie PD, et al. Zebrafish as a model for caveolin-associated muscle disease; caveolin-3 is required for myofibril organization and muscle cell patterning. *Hum Mol Genet*. 2005; 14: 1727–1743. doi: [10.1093/hmg/ddi179](https://doi.org/10.1093/hmg/ddi179) PMID: [15888488](https://pubmed.ncbi.nlm.nih.gov/15888488/)
25. Parton RG, del Pozo MA. Caveolae as plasma membrane sensors, protectors and organizers. *Nat Rev Mol Cell Biol*. 2013; 14: 98–112. doi: [10.1038/nrm3512](https://doi.org/10.1038/nrm3512) PMID: [23340574](https://pubmed.ncbi.nlm.nih.gov/23340574/)
26. Briand N, Dugail I, Le Lay S. Cavin proteins: New players in the caveolae field. *Biochimie*. 2011; 93: 71–77. doi: [10.1016/j.biochi.2010.03.022](https://doi.org/10.1016/j.biochi.2010.03.022) PMID: [20363285](https://pubmed.ncbi.nlm.nih.gov/20363285/)
27. Ogata T, Ueyama T, Isodono K, Tagawa M, Takehara N, Kawashima T, et al. MURC, a Muscle-Restricted Coiled-Coil Protein That Modulates the Rho/ROCK Pathway, Induces Cardiac Dysfunction and Conduction Disturbance. *Mol Cell Biol*. 2008; 28: 3424–3436. doi: [10.1128/MCB.02186-07](https://doi.org/10.1128/MCB.02186-07) PMID: [18332105](https://pubmed.ncbi.nlm.nih.gov/18332105/)
28. Tagawa M, Ueyama T, Ogata T, Takehara N, Nakajima N, Isodono K, et al. MURC, a muscle-restricted coiled-coil protein, is involved in the regulation of skeletal myogenesis. *Am J Physiol—Cell Physiol*. 2008; 295: C490–C498. doi: [10.1152/ajpcell.00188.2008](https://doi.org/10.1152/ajpcell.00188.2008) PMID: [18508909](https://pubmed.ncbi.nlm.nih.gov/18508909/)
29. Bastiani M, Liu L, Hill MM, Jedrychowski MP, Nixon SJ, Lo HP, et al. MURC/Cavin-4 and cavin family members form tissue-specific caveolar complexes. *J Cell Biol*. 2009; 185: 1259–1273. doi: [10.1083/jcb.200903053](https://doi.org/10.1083/jcb.200903053) PMID: [19546242](https://pubmed.ncbi.nlm.nih.gov/19546242/)
30. Ogata T, Naito D, Nakanishi N, Hayashi YK, Taniguchi T, Miyagawa K, et al. MURC/Cavin-4 facilitates recruitment of ERK to caveolae and concentric cardiac hypertrophy induced by α 1-adrenergic receptors. *Proc Natl Acad Sci*. 2014; 111: 3811–3816. doi: [10.1073/pnas.1315359111](https://doi.org/10.1073/pnas.1315359111) PMID: [24567387](https://pubmed.ncbi.nlm.nih.gov/24567387/)
31. Kovtun O, Tillu VA, Jung W, Leneva N, Ariotti N, Chaudhary N, et al. Structural Insights into the Organization of the Cavin Membrane Coat Complex. *Dev Cell*. 2014; 31: 405–419. doi: [10.1016/j.devcel.2014.10.002](https://doi.org/10.1016/j.devcel.2014.10.002) PMID: [25453557](https://pubmed.ncbi.nlm.nih.gov/25453557/)
32. Housley MP, Reischauer S, Dieu M, Raes M, Stainier DYR, Vanhullebeke B. Translational profiling through biotinylation of tagged ribosomes in zebrafish. *Dev Camb Engl*. 2014; 141: 3988–3993. doi: [10.1242/dev.111849](https://doi.org/10.1242/dev.111849)
33. Doyle EL, Booher NJ, Standage DS, Voytas DF, Brendel VP, VanDyk JK, et al. TAL Effector-Nucleotide Targeter (TALE-NT) 2.0: tools for TAL effector design and target prediction. *Nucleic Acids Res*. 2012; 40: W117–W122. doi: [10.1093/nar/gks608](https://doi.org/10.1093/nar/gks608) PMID: [22693217](https://pubmed.ncbi.nlm.nih.gov/22693217/)
34. Cermak T, Doyle EL, Christian M, Wang L, Zhang Y, Schmidt C, et al. Efficient design and assembly of custom TALEN and other TAL effector-based constructs for DNA targeting. *Nucleic Acids Res*. 2011; 39: e82–e82. doi: [10.1093/nar/gkr218](https://doi.org/10.1093/nar/gkr218) PMID: [21493687](https://pubmed.ncbi.nlm.nih.gov/21493687/)

35. Hamer P, McGeachie J, Davies M, Grounds M, Evans Blue Dye as an in vivo marker of myofibre damage: optimising parameters for detecting initial myofibre membrane permeability. *J Anat.* 2002; 200: 69–79. doi: [10.1046/j.0021-8782.2001.00008.x](https://doi.org/10.1046/j.0021-8782.2001.00008.x) PMID: [11837252](https://pubmed.ncbi.nlm.nih.gov/11837252/)
36. Jacoby AS, Busch-Nentwich E, Bryson-Richardson RJ, Hall TE, Berger J, Berger S, et al. The zebrafish dystrophic mutant softy maintains muscle fibre viability despite basement membrane rupture and muscle detachment. *Development.* 2009; 136: 3367–3376. doi: [10.1242/dev.034561](https://doi.org/10.1242/dev.034561) PMID: [19736328](https://pubmed.ncbi.nlm.nih.gov/19736328/)
37. Bassett DI, Bryson-Richardson RJ, Daggett DF, Gautier P, Keenan DG, Currie PD. Dystrophin is required for the formation of stable muscle attachments in the zebrafish embryo. *Development.* 2003; 130: 5851–5860. doi: [10.1242/dev.00799](https://doi.org/10.1242/dev.00799) PMID: [14573513](https://pubmed.ncbi.nlm.nih.gov/14573513/)
38. Hayashi YK, Matsuda C, Ogawa M, Goto K, Tominaga K, Mitsunashi S, et al. Human PTRF mutations cause secondary deficiency of caveolins resulting in muscular dystrophy with generalized lipodystrophy. *J Clin Invest.* 2009; 119: 2623–2633. doi: [10.1172/JCI38660](https://doi.org/10.1172/JCI38660) PMID: [19726876](https://pubmed.ncbi.nlm.nih.gov/19726876/)
39. Hansen CG, Shvets E, Howard G, Riento K, Nichols BJ. Deletion of cavin genes reveals tissue-specific mechanisms for morphogenesis of endothelial caveolae. *Nat Commun.* 2013; 4: 1831. doi: [10.1038/ncomms2808](https://doi.org/10.1038/ncomms2808) PMID: [23652019](https://pubmed.ncbi.nlm.nih.gov/23652019/)
40. Shyu K, Cheng W, Wang B, Chang H. Hypoxia activates muscle-restricted coiled-coil protein (MURC) expression via transforming growth factor- β in cardiac myocytes. *Clin Sci.* 2014; 126: 367–375. doi: [10.1042/CS20130260](https://doi.org/10.1042/CS20130260) PMID: [24001173](https://pubmed.ncbi.nlm.nih.gov/24001173/)
41. Mann CJ, Perdiguero E, Kharraz Y, Aguilar S, Pessina P, Serrano AL, et al. Aberrant repair and fibrosis development in skeletal muscle. *Skelet Muscle.* 2011; 1: 21. doi: [10.1186/2044-5040-1-21](https://doi.org/10.1186/2044-5040-1-21) PMID: [21798099](https://pubmed.ncbi.nlm.nih.gov/21798099/)
42. Rodgers JT, King KY, Brett JO, Cromie MJ, Charville GW, Maguire KK, et al. mTORC1 controls the adaptive transition of quiescent stem cells from G0 to GAlert. *Nature.* 2014; 510: 393–396. doi: [10.1038/nature13255](https://doi.org/10.1038/nature13255) PMID: [24870234](https://pubmed.ncbi.nlm.nih.gov/24870234/)
43. Volonte D, Peoples AJ, Galbiati F. Modulation of Myoblast Fusion by Caveolin-3 in Dystrophic Skeletal Muscle Cells: Implications for Duchenne Muscular Dystrophy and Limb-Girdle Muscular Dystrophy-1C. *Mol Biol Cell.* 2003; 14: 4075–4088. doi: [10.1091/mbc.E03-03-0161](https://doi.org/10.1091/mbc.E03-03-0161) PMID: [14517320](https://pubmed.ncbi.nlm.nih.gov/14517320/)
44. Lo HP, Nixon SJ, Hall TE, Cowling BS, Ferguson C, Morgan GP, et al. The caveolin–cavin system plays a conserved and critical role in mechanoprotection of skeletal muscle. *J Cell Biol.* 2015; 210: 833–849. doi: [10.1083/jcb.201501046](https://doi.org/10.1083/jcb.201501046) PMID: [26323694](https://pubmed.ncbi.nlm.nih.gov/26323694/)
45. Hayashi T, Arimura T, Ueda K, Shibata H, Hohda S, Takahashi M, et al. Identification and functional analysis of a caveolin-3 mutation associated with familial hypertrophic cardiomyopathy. *Biochem Biophys Res Commun.* 2004; 313: 178–184. doi: [10.1016/j.bbrc.2003.11.101](https://doi.org/10.1016/j.bbrc.2003.11.101) PMID: [14672715](https://pubmed.ncbi.nlm.nih.gov/14672715/)
46. Vatta M, Ackerman MJ, Ye B, Makielski JC, Ughanze EE, Taylor EW, et al. Mutant Caveolin-3 Induces Persistent Late Sodium Current and Is Associated With Long-QT Syndrome. *Circulation.* 2006; 114: 2104–2112. doi: [10.1161/CIRCULATIONAHA.106.635268](https://doi.org/10.1161/CIRCULATIONAHA.106.635268) PMID: [17060380](https://pubmed.ncbi.nlm.nih.gov/17060380/)
47. Catteruccia M, Sanna T, Santorelli FM, Tessa A, Giacompo RD, Sauchelli D, et al. Rippling muscle disease and cardiomyopathy associated with a mutation in the CAV3 gene. *Neuromuscul Disord.* 2009; 19: 779–783. doi: [10.1016/j.nmd.2009.08.015](https://doi.org/10.1016/j.nmd.2009.08.015) PMID: [19773168](https://pubmed.ncbi.nlm.nih.gov/19773168/)
48. Woodman SE, Park DS, Cohen AW, Cheung MW-C, Chandra M, Shirani J, et al. Caveolin-3 Knock-out Mice Develop a Progressive Cardiomyopathy and Show Hyperactivation of the p42/44 MAPK Cascade. *J Biol Chem.* 2002; 277: 38988–38997. doi: [10.1074/jbc.M205511200](https://doi.org/10.1074/jbc.M205511200) PMID: [12138167](https://pubmed.ncbi.nlm.nih.gov/12138167/)
49. Rodriguez G, Ueyama T, Ogata T, Czernuszewicz G, Tan Y, Dorn GW, et al. Molecular Genetic and Functional Characterization Implicate Muscle-Restricted Coiled-Coil Gene (MURC) as a Causal Gene for Familial Dilated Cardiomyopathy. *Circ Cardiovasc Genet.* 2011; 4: 349–358. doi: [10.1161/CIRCGENETICS.111.959866](https://doi.org/10.1161/CIRCGENETICS.111.959866) PMID: [21642240](https://pubmed.ncbi.nlm.nih.gov/21642240/)
50. Rappsilber J, Ishihama Y, Mann M. Stop and Go Extraction Tips for Matrix-Assisted Laser Desorption/Ionization, Nanoelectrospray, and LC/MS Sample Pretreatment in Proteomics. *Anal Chem.* 2003; 75: 663–670. doi: [10.1021/ac026117i](https://doi.org/10.1021/ac026117i) PMID: [12585499](https://pubmed.ncbi.nlm.nih.gov/12585499/)
51. Bolstad BM, Irizarry RA, Åstrand M, Speed TP. A comparison of normalization methods for high density oligonucleotide array data based on variance and bias. *Bioinformatics.* 2003; 19: 185–193. doi: [10.1093/bioinformatics/19.2.185](https://doi.org/10.1093/bioinformatics/19.2.185) PMID: [12538238](https://pubmed.ncbi.nlm.nih.gov/12538238/)